Photoacoustics 42 (2025) 100702

Contents lists available at ScienceDirect

Photoacoustics

journal homepage: www.elsevier.com/locate/pacs

# A sulfur dioxide detection platform based on photoacoustic spectroscopy and a 266.22 nm high-power stabilized LD-pumped solid-state Q-switched laser

Xiaowen Shen [a,b,1], Yixin Zhang [a,b,1], Ruyue Cui [a,b,1], Donghe Tian [c], Ming Cheng [c], Pietro Patimisco [a,d], Angelo Sampaolo [a,d], Chaofeng Sun [a,b], Xukun Yin [e], Vincenzo Spagnolo [a,d,*], Lei Dong [a,b,d,*], Hongpeng Wu [a,b,d,*]

[a] State Key Laboratory of Quantum Optics and Quantum Optics Devices, Institute of Laser Spectroscopy, Shanxi University, Taiyuan 030006, PR China
[b] Collaborative Innovation Center of Extreme Optics, Shanxi University, Taiyuan 030006, PR China
[c] Changchun New Industries Optoelectronics Technology Co., Ltd, PR China
[d] PolySense Lab-Dipartimento Interateneo di Fisica, University and Politecnico of Bari, Via Amendola 173, Bari, Italy
[e] Hangzhou Institute of Technology, Xidian University, Hangzhou 311231, PR China

ARTICLE INFO

*Keywords:*
Photoacoustic spectroscopy
Trace gas sensor
Sulfur dioxide
Outdoor real-time detection

ABSTRACT

A ppb-level sulfur dioxide ($SO_2$) monitoring platform was developed by exploiting standard photoacoustic spectroscopy and a novel, highly stable UV laser. A 266.22 nm LD-pumped solid-state, acousto-optic modulator Q-switched laser with high beam quality ($M^2$ =1.0275) and excellent output optical power stability ($\delta_{P\sigma}$ < 1 % ~24 h) was selected as light source of the photoacoustic sensor. The performance of the $SO_2$ sensor was evaluated in terms of gas flow rate, pressure, and detection sensitivity. An ultimate detection limit of 3 ppb for $SO_2$ detection in $N_2$ was demonstrated with 1 s integration time, in laboratory environment. Continuous outdoor monitoring for five days verified the excellent stability and reliability of the reported $SO_2$ photoacoustic sensor.

## 1. Introduction

Sulfur dioxide ($SO_2$) is considered one of the major atmospheric pollutant due to its conversion to sulfate aerosol particles in the lower atmosphere, which are precursors to environmental acidification. The International Agency for Research on Cancer (IARC) of the World Health Organization classifies $SO_2$ as Group 3 of carcinogens. At concentrations of a few part-per million, $SO_2$ affects the human body causing serious irritation. When it reaches 8 ppm, it may lead to coughing symptoms. The $SO_2$ effects on human body are exacerbated when it is present simultaneously with atmospheric soot. For example, a sub-ppm $SO_2$ concentration together with a concentration of soot exceeding 0.106 ppm in atmosphere, enhance the risk of respiratory diseases and the condition of patients with chronic illnesses may deteriorate rapidly. Prolonged exposure to high concentrations of $SO_2$ can cause respiratory, cardiovascular, immune system disorders, and in severe cases, even be life-threatening [1–3].

$SO_2$ is commonly used in industry as a catalyst, dehydrating agent, and bleaching agent, as well as in the production of chemicals such as sulfuric acid, phosphoric acid, and sulfates [4–6]. It is also used as a fuel additive to improve combustion efficiency and reduce emissions [7]. In high-voltage power systems, the inert gas $SF_6$ can produce $SO_2$ during corona discharge and spark decomposition. Different $SO_2$ concentrations can reflect different insulation defects within the GIS, leading to power system failures and serious accidents [8]. Consequently, monitoring and controlling $SO_2$ is crucial in atmospheric monitoring, public health, and industrial applications.

Photoacoustic Spectroscopy (PAS) is a widely used gas detection technique due to its high sensitivity, selectivity, fast response, and low cost [9–16]. The basic theory of PAS is that target molecules are excited by the absorption of modulated or pulsed light at a wavelength resonant with a roto-vibrational radiative transition. The thermal energy released by non-radiative relaxation processes of excited molecules causes localized transient thermal expansion of the target gas, thus generating

* Corresponding authors at: State Key Laboratory of Quantum Optics and Quantum Optics Devices, Institute of Laser Spectroscopy, Shanxi University, Taiyuan 030006, PR China.
*E-mail addresses:* vincenzoluigi.spagnolo@poliba.it (V. Spagnolo), donglei@sxu.edu.cn (L. Dong), wuhp@sxu.edu.cn (H. Wu).
[1] These authors contributed equally to this paper

https://doi.org/10.1016/j.pacs.2025.100702
Received 30 January 2025; Received in revised form 17 February 2025; Accepted 18 February 2025
Available online 18 February 2025

acoustic or ultrasonic waves at the modulation or pulse frequency of the light. Acoustic wave is detected by a broadband microphone (standard PAS) [17,18] or quartz tuning fork (QEPAS) [19–24]or by a cantilever (CEPAS) [25]. In all three cases, the electrical signal generated by the acousto-electric transducer will be proportional to the target gas concentration. PAS technology has been widely used for $SO_2$ detection in recent years, targeting an $SO_2$ absorption feature properly selected within its strong absorption mid-infrared band in the spectral range 7.2–7.6 μm. In 2014, J. P. Waclawek et al. used a mid-infrared distributed feedback quantum cascade laser (DFB-QCL) operating at 7.24 μm in a QEPAS sensor to detect $SO_2$ in humidi6-fied $N_2$ matrix, achieving a minimum detection limit (MDL) of 63 ppb with a 1 s integration constant [26]. In 2020, X. Yin et al. reached an MDL of 2.45 ppb using a 7.41 μm high-power QCL in a PAS sensor [27]. Although $SO_2$ exhibits the strongest absorption band in the mid-infrared range, this spectral window may not be the best choice for the operation of a $SO_2$ sensor in industrial applications because other resulting gases from industrial processes, such as $SF_6$, also have strong absorption lines in the mid-infrared range. Therefore, several works explored also the use of strong $SO_2$ absorption bands in the UV range as listed in the MPI-Mainz database [28,29]. The interest in targeting UV absorption bands has been also triggered by recent developments in innovative UV sources. UV lasers are divided into three types: solid-state lasers, gas lasers and semiconductor lasers. Due to their high efficiency, reliable performance and simple hardware structure, the new semiconductor-pumped all-solid-state lasers in the short-wavelength UV band have a wide range of applications, including trace gas sensing. In 2001, M. A. Gondal et al. achieved an MDL of 1.3 ppb for $SO_2$ detection in $N_2$ using a 225.7 nm pulsed laser [30]. In 2017, X. Yin et al. used a 303 nm UV-band diode-pumped solid-state laser with an output power of 5 mW to achieve an MDL of 74 ppb for $SO_2$ detection in an $SF_6$ matrix [31]. Working with the same gas matrix, in 2023 B. Chen et al. used a passive Q-switching laser diode (LD) pumped all-solid-state 266.22 nm deep-ultraviolet laser to achieve an MDL of 140 ppb [32]. The main drawback of the laser sources in the UV range is related to the laser power fluctuations which compromise the long-term stability of the $SO_2$ sensor response.

In this study, a 266.22 nm LD-pumped all-solid-state, acousto-optic modulator, Q-switched UV laser was used as the excitation light source for the $SO_2$ detection in a PAS sensor. This laser has high output power and long-term stability, which breaks through the strict requirement of laser power monitoring during sensor operation to compensate the laser power fluctuations on the PAS signal. The PAS sensor was tested for long-term detection of atmospheric $SO_2$ with a high sensitivity and selectivity.

## 2. Selection of $SO_2$ absorption wavelength

Together with $SF_6$ and its derivatives (e.g. $SO_2$ and $H_2S$), other atmospheric pollutant gases (e.g. NO and $NO_2$) also have absorption bands in the UV spectral range (10 nm - 400 nm). The absorption spectra of these atmospheric pollutant gases are simulated in Fig. 1 by using the MPI-Mainz database yielded.

The vacuum-ultraviolet region 10–200 nm cannot be targeted by optical sources. Two distinct $SO_2$ absorption bands lie in the near-ultraviolet region 200–400 nm. In this range, the absorption of $SF_6$ gas is negligible, and water vapor, $NO_2$, $N_2O$, and $H_2S$ have weak spectral interfere with the $SO_2$ absorption band. The strongest $SO_2$ absorption lines fall in the 200–225 nm range. however, the significant spectral overlap with the $H_2S$ band prevents a selective $SO_2$ detection. Therefore, the 266.22 nm absorption line in the 250–350 nm band was selected as a good compromise between high absorption cross section and weak spectral overlap with other interferents. In previous studies [32] the same line at 266.22 nm was targeted by using a laser source with output power stability of 0.04 % in 2 h of operation, reaching an ultimate detection limit of 140 ppb for $SO_2$ detection in the $SF_6$ matrix. However,

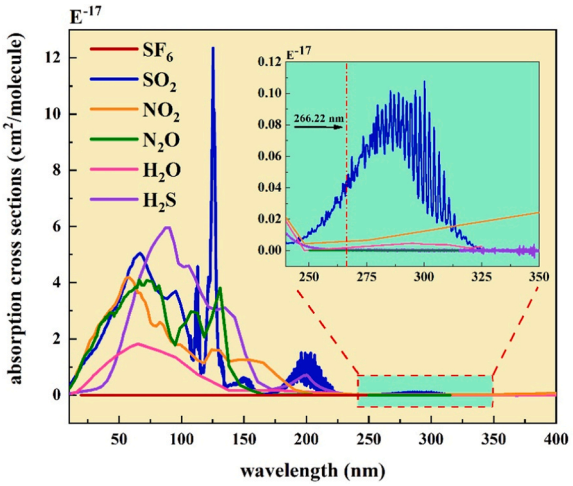


**Fig. 1.** $SO_2$ absorption cross-sections (blue line) simulated in the spectral range 10–400 nm by using the MPI-Mainz database, at room temperature and atmospheric pressure. Absorption cross-sections of $SF_6$, $NO_2$, $N_2O$, $H_2O$ and $H_2S$ are also reported in the same spectral range.

sensor performance starts to deteriorate when operation is extended for longer times, mainly due to optical power instability.

## 3. $SO_2$ gas photoacoustic sensing monitoring platform

The $SO_2$ PAS sensor employing a novel UV laser optical source with acousto-optic active Q-modulation technology is shown in Fig. 2. The core component is a high Q-factor photoacoustic cell (PAC) made of stainless steel with the inner surfaces finely polished to reduce surface loss. Two quartz windows (Φ25.4 × 5 mm) are fitted for laser in and out. An LD-pumped all-solid-state laser is pulse-modulated by a function generator (Tektronix, AFG31052) to provide a stable modulated outup at 266.22 nm. The laser beam passes through the PAC filled with $SO_2$ gas sample to excite the photoacoustic effect by resonant optical absorption from $SO_2$ molecules. The generated weak acoustic waves are detected by a high sensitivity microphone placed within the PAC. The electrical signal generated by the microphone is demodulated at the laser pulse frequency (1 *f* detection) by a lock-in amplifier (Stanford Research Systems, SR830), with the filter slope set to 12 dB/oct and the time constant to 1 sec, triggered by a reference signal provided by the function generator. A power meter (Ophir Photonics, 3A-FS & Nova II) is placed at the PAC exit to monitor the transmitted laser beam in real-time.

A gas dilution system (Environics, EN4000) equipped with two mass flow controllers was used to generate different $SO_2$: $N_2$ gas mixtures ranging from 0 to 50 ppm. A pressure controller and a system of needle valves (NV), as well as a gas flow meter and a diaphragm pump (KNF Neuberger GmbH, N813.5ANE) both placed downstrain, complete the gas handling system for precise control and measurement of the pressure and gas flow inside the gas line. All experiments were conducted at atmospheric pressure and room temperature to ensure the accuracy and reliability of the results.

## 4. Parameter optimization and performance evaluation of UV lasers

In the experiment, a Changchun New Industries' AO-Mini-E-266 (20 mW) LD-pumped all-solid-state laser with an Acousto-optic modulator (AOM) was used. This laser uses a semiconductor pump source to efficiently transfer the pump source to the gain medium, thereby creating population inversion and consequently light at the fundamental frequency. AOM Q-switching is used to obtain pulses with an adjustable repetition rate, to be then amplified by Raman scattering. Finally,

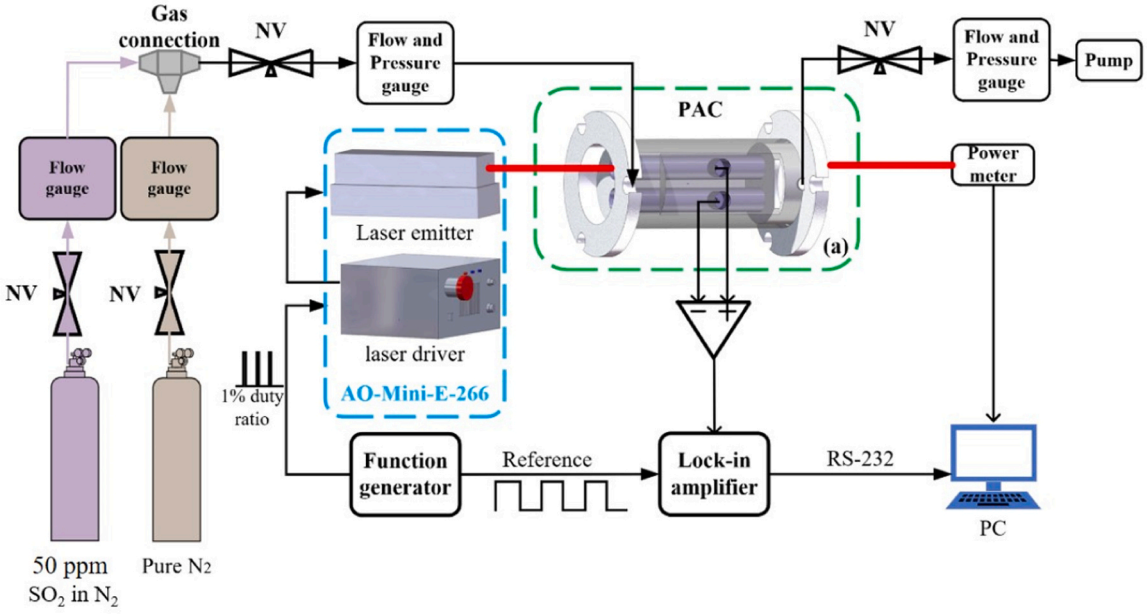


**Fig. 2.** Schematic of the photoacoustic sensor for $SO_2$ detection. NV: Needle valve; PAC: photoacoustic cell.

nonlinear crystals for frequency doubling and quadrupling are used to convert them into monochromatic UV pulsed light at specific repetition rate, with stable output power and good spatial beam quality. These features make it suitable as light source in a PAS sensor for trace gas detection.

The main characteristics of the output UV laser beam were measured at first. According to the national standards specified in Measurement methods for the main parameters of solid-state lasers (GB/T 15175–2012), the laser beam spatial quality is mainly characterized by the following features: beam waist diameter ($d_0$, mm), far-field beam scattering angle ($\theta$, mrad), and beam quality factor ($M^2$), which related by:

$$M^2 = \frac{\pi}{4\lambda} \bullet d_0 \bullet \theta \tag{1}$$

With an emission wavelength of 266.22 nm, the repetition frequency and the duty cycle were set to 1773 Hz and 1 %, respectively, resulting

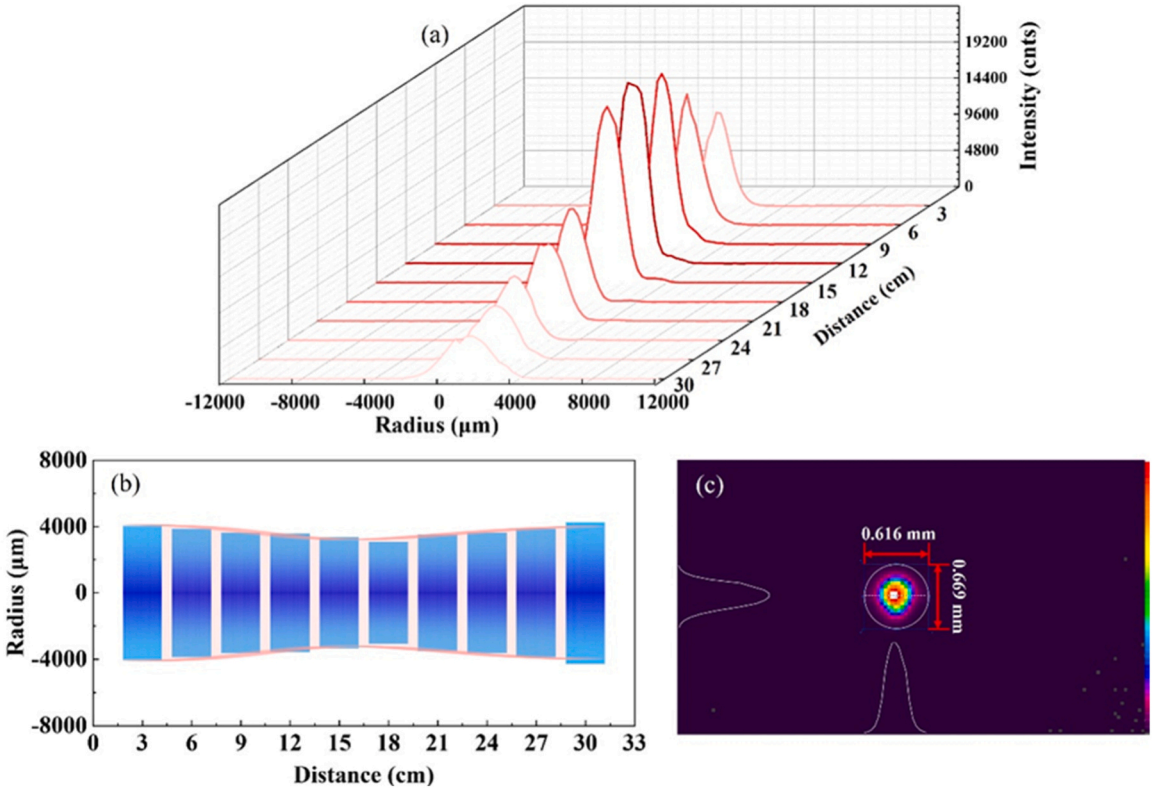


**Fig. 3.** (a) Intensity distribution of LD-pumped all-solid-state UV laser beam acquired at different distances; (b) Laser beam radius as a function of the distance; (c) Two-dimensional intensity distribution of the UV laser beam acquired 18 cm far from the laser source.

in an output optical power of 17.6 mW. The repetition rate of the laser was set to match the resonance frequency of the photoacoustic cell. This is because the photoacoustic cell used in this experiment is a resonant-type cell, which can efficiently detect acoustic signals only when their frequency matches its resonance frequency. The intensity distribution of the laser beam was reconstructed by a pyrocamera (Ophir Photonics, PY-III-HR-C-A-Pro, Camera), by placing the it at different distances from the laser source, from 3 cm to 30 cm at steps of 3 cm. Fig. 3(a) shows the laser intensity distribution as the distance increases from 3 cm to 30 cm.

For each profile, the beam size was extracted by measuring the radial distances at which the light intensity drops to $1/e^2$ of its maximum central value by fitting the profiles with a Gaussian function. Fig. 3(b) reports the extracted beam radius as a function of the pyrocamera distance. The beam propagation in the investigated pathlength can be considered as an approximation of a parallel beam in the Rayleigh range. Fig. 3(c) reports the intensity distribution corresponding to the lowest sizes, achieved when the camera is positioned 18 cm far from the laser source. At this distance, the beam diameter ($d_0$) is 0.616 mm and 0.669 mm along x- and y-direction, respectively, with a far-field beam scattering angle(θ) of 0.54 mrad. By using Eq. (1), $M^2$ results 1.028, indicating that the beam quality resembles that of a theoretical diffraction-limited Gaussian beam.

A key performance metric for laser manufacturing is the power stability. The output beam power stability of solid-state lasers is mainly characterized by the two figures of merit, the Peak-to-Peak Stability (PTP Std) and the Output power stability. PTP Std, characterizing the range of output power variation over a specific period of time, indicates the percentage spread between the highest ($P_{Max}$) and lowest ($P_{Min}$) power values measured over a set of $N$ continuous measurements, as:

$$PTP\ Std = \frac{\frac{P_{Max}-P_{Min}}{2}}{P_{ave}} \times 100\% \quad (2)$$

where $P_{ave}$ is the average power. The output power stability characterizes the degree of dispersion of the output power with respect to the mean value. It is usually expressed in terms of the output power standard deviation instability ($\delta_{P\sigma}$) as:

$$\delta_{P_\sigma} = \frac{kP_\sigma}{P_{ave}} \times 100\% \quad (3)$$

where, $k = 1, 2, 3\ldots$ is the coefficient of standard deviation and $P_\sigma$ is the power standard deviation defined as:

$$P_\sigma = \sqrt{\frac{\sum_{i=1}^{N}(P_i - P_{ave})}{N-1}} \quad (4)$$

To long-term monitor the output laser power, the power meter was placed at the exit of the PAC filled with a 50 ppm $SO_2$: $N_2$ gas mixture. Fig. 4 displays the laser power monitoring data over 24 h.

An average optical power of $P_{ave}$= 17.6 mW was measured, with $P_{Max} - P_{Min}$ = 0.75 mW. From Eq. (3), *PTP Std* results 2.13 %. The standard deviation of the output power instability can be calculated by using Eq. (4) with k = 1, and results $\delta_{P\sigma}$ = 0.212 % over 4 h and $\delta_{P\sigma}$ = 0.853 % over 24 h. For both short and long temporal dynamic domain, $\delta_{P\sigma}$ values calculated are less than 1 %, and are mainly due to the thermal fluctuations of the crystal inside the laser. However, the performance test results demonstrate the high-quality output beam as well as the long-term power stability makes the laser source as an excellent candidate for PAS spectroscopy.

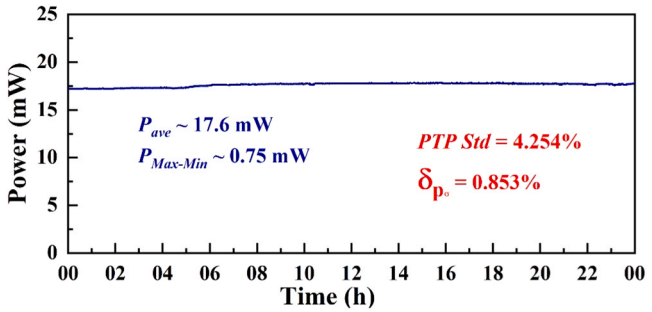


**Fig. 4.** Optical power monitoring of UV laser output over a 24-Hour period.

## 5. Parameter optimization and performance evaluation

The gas flow rate significantly affects the time required for gas exchange within the photoacoustic cell, thereby altering the overall response time of the sensor. However, while a higher flow rate decreases the response time, it may also increase the background noise of the system. Therefore, the effect of gas flow rate on sensor performance was initially investigated. Additionally, considering the adhesive properties of $SO_2$ gas, the temperature of the gas entering the photoacoustic cell was monitored during flow rate optimization. In this study, the gas temperature was consistently maintained at room temperature, 24℃. Both flow rate and temperature data were continuously recorded in real time using gas flow meters (Alicat Scientific, Inc. Model M-500SCCM-D, UK). To verify the influence of flow rate on $SO_2$ sensor performance, the PAS signal was measured by injected a certified mixture of 50 ppm $SO_2$: $N_2$ in the PAC at different flow rates. Fig. 5(a) reports the PAS signal amplitude acquired at different flow rates at atmospheric pressure, together with that acquired when pure $N_2$ is injected in the PAC.

Increasing the flow rate from 100 Sccm to 600 Sccm does not significantly change the signal level when pure $N_2$ was injected into the PAC. This indicates that the increase in flow rate did not introduce additional background noise. Conversely, with the mixture of 50 ppm $SO_2$:$N_2$, the PAS signal amplitude gradually increases as the flow rate was increased from 100 to 300 Sccm. At higher flow rates up to 600 Sccm, no significant increase in signal amplitude was observed. Thus, all measurements reported hereafter will be performed at 300 Sccm. Being the volume of the PAC approximately of 9.8 ml, this corresponds to a gas exchange time of ~ 2 s.

Changes in the gas pressure within the photoacoustic cell not only alter the resonance frequency and quality factor of the cell but also affect the photoacoustic relaxation rate of the gas, thereby significantly changing the amplitude of the photoacoustic signal. When investigating the impact of gas pressure on sensor performance, the resonance frequency of the photoacoustic cell at different pressures is first tested. Then, the laser modulation frequency is set to match the respective resonance frequency before measuring the photoacoustic signal. Fig. 5 (b) reports the PAS signal amplitude as a function of the gas pressure. The signal varies linearly as the pressure increases, thus atmospheric pressure was selected as the optimal one for all measurements.

To assess the sensitivity of the PAS sensor for $SO_2$ detection, different mixtures were injected with $SO_2$ concentrations ranging from 0 to 5 ppm in $N_2$ matrix. Stepwise $SO_2$ concentration measurements were performed to verify the linearity of the PAS signal as a function of the $SO_2$ concentration. For each concentration step, the PAS signal was measured every 1 s, for a total time duration of ~ 28 min. The results are shown in Fig. 6(a). Considering the gas exchange time, for each step, when the $SO_2$ concentration is varied, a dead time of 2 s was considered before starting the PAS signal acquisition.

For each concentration step, data were averaged and plotted as a function of the $SO_2$ concentration to obtain the calibration curve shown in Fig. 6(b). The results confirm that the PAS signal is proportional to the $SO_2$ concentration with a sensitivity of 0.44 mV/ppm. Considering a noise level of 0.10 mV, a minimum detection limit of ~3 ppb was estimate [33,34].

To further verify the detection performance of the $SO_2$ photoacoustic spectroscopy sensor, an online monitoring study of atmospheric $SO_2$ concentrations was conducted outdoors. Since the resonance frequency

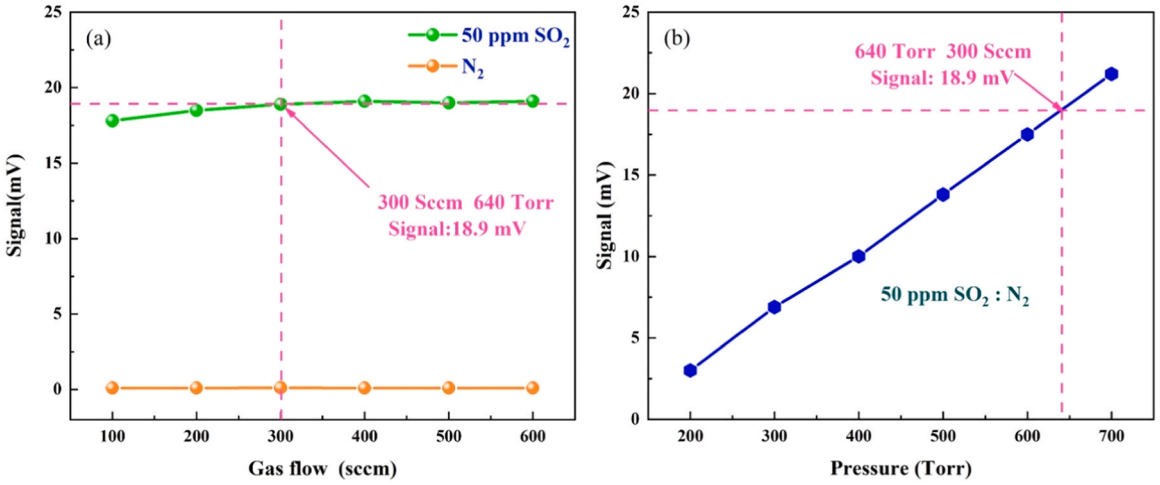


**Fig. 5.** (a) PAS signals for 50 ppm $SO_2$ (green) and pure $N_2$ (orange) at various mass flow rates. (b) PAS signal amplitude vs. gas pressure (200–700 Torr) for 50 ppm $SO_2$ at 300 Sccm.

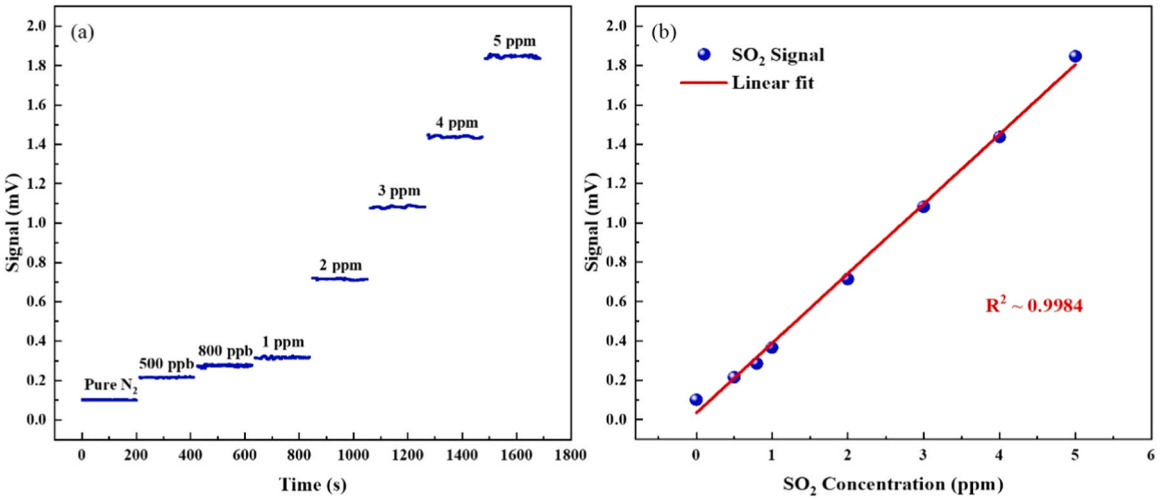


**Fig. 6.** (a) Stepwise $SO_2$:$N_2$ PAS signal amplitudes at 500 ppb – 5 ppm. (b) Calibration curve from measured PAS signals vs. $SO_2$ concentration.

of the photoacoustic cell shifts with changes in the gas density inside the resonator cavity, it is necessary to recalibrate the resonance frequency of the photoacoustic cell prior to outdoor monitoring.

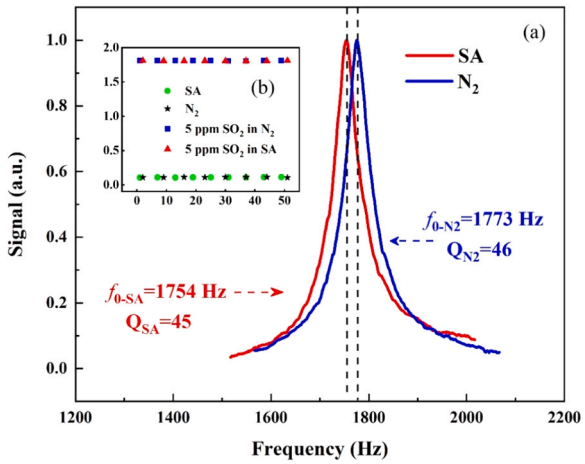


**Fig. 7.** (a) The frequency response curves of the differential photoacoustic cell in $N_2$ and SA. (b) Influence of carrier gas on $SO_2$ signal.

As shown in Fig. 7(a), the resonance frequency of the photoacoustic cell in synthetic air (SA) and $N_2$ were $f_0$= 1754 Hz and $f_0$= 1773 Hz, the full width at half maximum (FWHM) of the resonance width were $\Delta f$ = 39 Hz and $\Delta f$ = 38 Hz, resulting in a Q-factor of 45 and 46, respectively.

The photoacoustic signals of 5 ppm $SO_2$ using SA (▲ symbols) and $N_2$ (■ symbols) as carrier gases are plotted in Fig. 7(b), with the laser modulation frequency set to 1754 Hz and 1773 Hz, respectively. The background noise of the sensor under both SA (● symbols) and $N_2$ (★ symbols) conditions were also measured at the laser modulation frequencies corresponding to their respective resonance frequencies. The nearly identical results of the data sets indicate that changing the carrier gas only affects the resonance frequency of the photoacoustic cell without significantly impacting its other characteristics. Therefore, when conducting atmospheric $SO_2$ concentration monitoring, all experimental parameters are kept as optimized in the previous section.

To test its potentiality for outdoor operation, the $SO_2$ PAS sensor platform was placed on the third floor of the First Laboratory in Taiyuan, Shanxi, in China. A 3 μm diameter PTFE microporous membrane was installed upstream at the air inlet of the PTFE tube to reduce the contamination of the PAC coming from dust and particulate matter present in the atmosphere. Fig. 8(a) shows the atmospheric $SO_2$ concentration continuously monitored between October 29, 2023, and

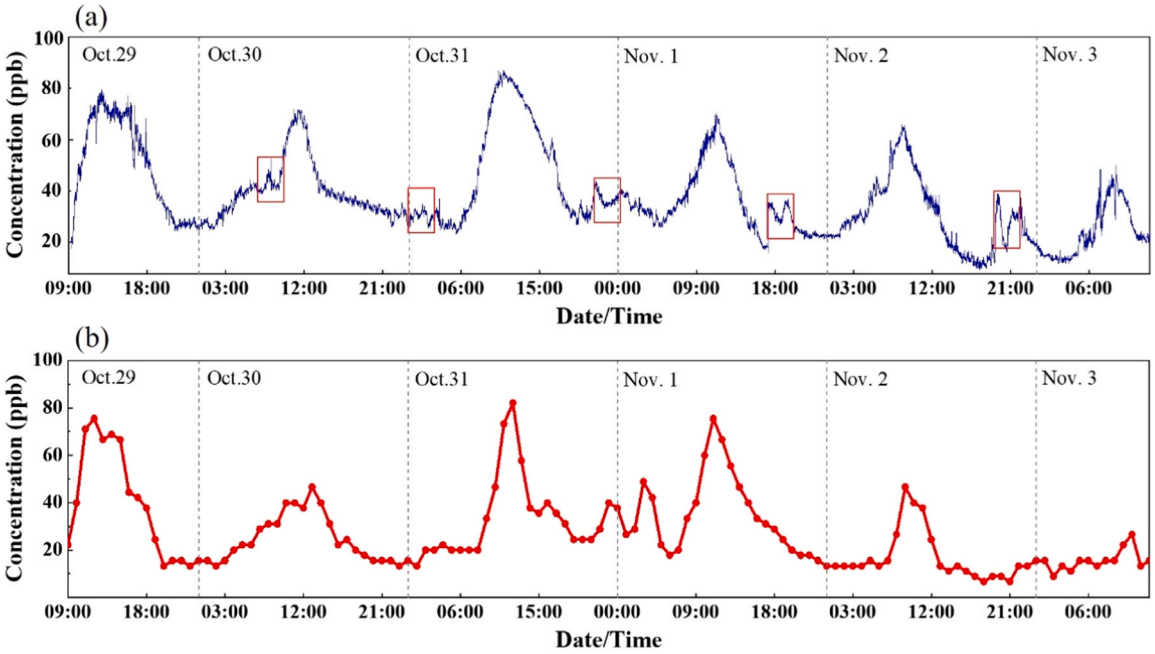


**Fig. 8.** (a) Real-time $SO_2$ monitoring at First Laboratory, Taiyuan (Oct. 29 - Nov. 3, 2023) using the developed PAS platform (blue). (b) Atmospheric $SO_2$ acquired by the Wucheng monitoring station of the China National Environmental Monitoring Center in the same time period.

November 3, 2023, at a 1 Hz acquisition rate. For comparison, Fig. 8(b) shows the atmospheric $SO_2$ recorded by the Wucheng monitoring station of the China National Environmental Monitoring Center (CNEMC). The Wucheng station is located ~ 3 km far from the PAS sensor, and the CNEMC platform updates its data every hour.

A good match between the two datasets can be observed, with a better reconstruction of the temporal variability of $SO_2$ trace by the PAS sensor because of its high refresh rate between two consecutive measurements. Each day, starting from ~9:00 a.m., the concentration of $SO_2$ gradually increases and reaches a peak at around 12:00 p.m.; then, it starts to decrease up to 18:00 p.m. and remains almost flat overnight. The increase in the morning can be correlated to air pollutant emissions from transportation as well as to emission of $SO_2$ gases caused by heating, charcoal, and cooking in northern China during the winter period. The remarkable differences between the two datasets are showed in red boxes in Fig. 8(a). One possible cause of the observed jitter is small fluctuations in the gas chamber caused by outside gases entering the chamber, another potential cause is laser output power jitter. As shown in Fig. 9, the laser power was monitored over a period of five days. The laser power undergoes automatic calibration approximately every 24–27 h, during which a certain amount of power fluctuation (both increases and decreases) is observed. This process leads to the fluctuations in the data marked by the red box in Fig. 8(a). However, these fluctuations do not have a significant impact on the overall concentration curve. Although some jitter appears on the timeline corresponding to the red box in Fig. 8(a), the output power remains stable at around 17 mW.

## 6. Conclusion

To address the issue of limited optical power stability and in turn unfeasibility for long-term monitoring, a $SO_2$ gas sensor based on photoacoustic spectroscopy and a novel, highly stable 266.22 nm-laser was developed. The sensing platform employs a UV laser with active acousto-optic Q-modulation technology, which has a high beam quality ($M^2 = 1.0275$) and a good stability of the output power ($\delta_{P\sigma} = 0.212\ \% < 1\ \%$ over 4 h, $\delta_{P\sigma} = 0.853\ \% < 1\ \%$ over 24 h) compared with the UV-band lasers previously investigated. To overcome the challenge of maintaining optical power stability in long-term monitoring, the sensor achieved a minimum detection limit (MDL, 1σ) of ~3 ppb at a steady excitation power of ~17 mW in a laboratory test of certified gas concentrations. Outdoor $SO_2$ monitoring was also performed for five consecutive days, and the test showed that the standard deviation of the laser output power for five consecutive days of monitoring was $\delta_{P\sigma} = 4.039\ \% < 5\ \%$, which meets the criteria for long term stability of lasers, and that the sensor matches very well with the data from the $SO_2$ monitor that passes through the monitoring station. This technology provides a solution with high stability and sensitivity for photoacoustic gas sensors, which is particularly suitable for environments requiring long-term monitoring and high-precision detection. In the future,

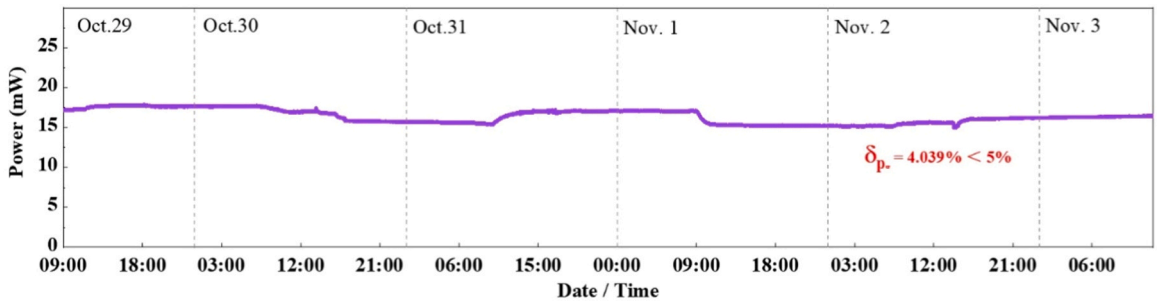


**Fig. 9.** Optical laser power monitoring from Oct. 29 to Nov. 3, 2023, during $SO_2$ platform operation. The x-axis timeline matches Fig. 8.

sensors based on this technology have a wide range of applications in environmental monitoring, industrial gas leakage detection, and gas monitoring in power systems.

## CRediT authorship contribution statement

**Zhang Yixin:** Methodology, Investigation, Data curation. **Shen Xiaowen:** Writing – original draft, Investigation, Data curation. **Patimisco Pietro:** Writing – review & editing, Methodology, Conceptualization. **Sampaolo Angelo:** Writing – review & editing, Methodology, Conceptualization. **Cheng Ming:** Writing – original draft, Methodology, Investigation. **Tian Donghe:** Writing – review & editing, Methodology, Conceptualization. **Cui Ruyue:** Writing – review & editing, Supervision, Methodology, Data curation. **Dong Lei:** Writing – review & editing, Supervision, Project administration, Methodology, Conceptualization. **Spagnolo Vincenzo:** Writing – review & editing, Supervision, Methodology, Funding acquisition, Conceptualization. **Yin Xukun:** Writing – review & editing, Methodology, Conceptualization. **Sun Chaofeng:** Writing – original draft, Investigation, Formal analysis, Conceptualization. **Wu Hongpeng:** Writing – review & editing, Supervision, Methodology, Funding acquisition, Conceptualization.

## Declaration of Competing interest

The authors declare that they have no known competing financial interests or personal relationships that could have appeared to influence the work reported in this paper

## Acknowledgments

The project is supported by National Natural Science Foundation of China (NSFC) [grant numbers 62475137, 62122045, 62075119, 62235010, 62175137, 62105252]; The Shanxi Science Fund for Distinguished Young Scholars (20210302121003). Authors from Hangzhou Institute of Technology acknowledge funding from Hangzhou Science and Technology Development Project (202204T04). Authors from PolySensSe Lab acknowledge funding from PNRR MUR project PE0000023-NQSTI; MUR – Dipartimenti di Eccellenza 2023–2027 – Quantum Sensing and Modelling for One-Health (QuaSiModO) and THORLABS GmbH within the PolySenSe joint research laboratory.

## Data availability

Data will be made available on request.

## References

[1] E.M. Khalaf, M.J. Mohammadi, S. Sulistiyani, A.A. Ramírez-Coronel, F. Kiani, A. T. Jalil, A.F. Almulla, P. Asban, M. Farhadi, M. Derikondi, Effects of sulfur dioxide inhalation on human health: a review, Rev. Environ. Health 39 (2022) 331–337.
[2] W.S. Tunnicliffe, M.F. Hilton, R.M. Harrison, J.G. Ayres, The effect of sulphur dioxide exposure on indices of heart rate variability in normal and asthmatic adults, *Eur. Respir.* J. 17 (2001) 604–608.
[3] X. Zhao, Y. Zhang, X. Han, H. Qi, F. Ma, K. Chen, Pressure-compensated fiber-optic photoacoustic sensors for trace $SO_2$ analysis in gas insulation equipment, Anal. Chem. 96 (2024) 10995–11001.
[4] K.H. Ng, S.Y. Lai, N.F.M. Jamaludin, A.R. Mohamed, A review on dry-based and wet-based catalytic sulphur dioxide ($SO_2$) reduction technologies, J. Hazard. Mater. 423 (2022) 127061.
[5] H. Zhang, M. Wang, X. Jiang, Sustainable access to sulfonic acids from halides and thiourea dioxide with air, Green. Chem. 22 (2020) 8238–8242.
[6] H. Qi, X. Zhao, Y. Xu, L. Yang, J. Liu, K. Chen, Rapid photoacoustic exhaust gas analyzer for simultaneous measurement of nitrogen dioxide and sulfur dioxide, Anal. Chem. 96 (2024) 5258–5264.
[7] T.N. Rhys-Jones, J.R. Nicholls, P. Hancock, Effects of $SO_2/SO_2$ on the efficiency with which MgO inhibits vanadic corrosion in residual fuel fired gas turbines, Corros. Sci. 23 (1983) 139–149.
[8] J. Luo, Y.H. Fang, Y.D. Zhao, A.J. Wang, D.C. Li, Y.Y. Li, J.X. Liu, Research on the detection of $SF_6$ decomposition products based on non-resonant photoacoustic spectroscopy, Anal. Methods 7 (2015) 1200–1207.
[9] K. Kinjalk, F. Paciolla, B. Sun, A. Zifarelli, G. Menduni, M. Giglio, H. Wu, L. Dong, D. Ayache, D. Pinto, A. Vicet, A. Baranov, P. Patimisco, A. Sampaolo, V. Spagnolo, Highly selective and sensitive detection of volatile organic compounds using long wavelength InAs-based quantum cascade lasers through quartz-enhanced photoacoustic spectroscopy, Appl. Phys. Rev. 11 (2024) 021427.
[10] C. Feng, B. Li, Y. Jing, J. Wang, P. Patimisco, V. Spagnolo, A. Sampaolo, L. Dong, H. Wu, Enrichment-enhanced photoacoustic spectroscopy based on vertical graphene, Sens. Actuators B Chem. 417 (2024) 136204.
[11] Y. Ma, Y. He, L. Zhang, X. Yu, J. Zhang, R. Sun, F.K. Tittel, Ultra-high sensitive acetylene detection using quartz-enhanced photoacoustic spectroscopy with a fiber amplified diode laser and a 30.72 kHz quartz tuning fork, Appl. Phys. Lett. 110 (2017) 03110.
[12] Z. Wang, Q. Wang, Y. Ching, J. Wu, G. Zhang, W. Ren, A portable low-power QEPAS-based $CO_2$ isotope sensor using a fiber-coupled interband cascade laser, Sens. Actuators B Chem. 246 (2017) 710–715.
[13] Q. Wang, Z. Wang, W. Ren, P. Patimisco, A. Sampaolo, V. Spagnolo, Fiber-ring laser intracavity QEPAS gas sensor using a 7.2 kHz quartz tuning fork, Sens. Actuators B Chem. 268 (2018) 512–518.
[14] H. Zheng, M. Lou, L. Dong, H. Wu, W. Ye, X. Yin, C.S. Kim, M. Kim, W.W. Bewley, C.D. Merritt, C.L. Canedy, M.V. Warren, I. Vurgaftman, J.R. Meyer, F.K. Tittel, Compact photoacoustic module for methane detection incorporating interband cascade light emitting device, Opt. Express 25 (2017) 16761–16770.
[15] C. Liu, G. Wang, C. Zhang, P. Patimisco, R. Cui, C. Feng, A. Sampaolo, V. Spagnolo, L. Dong, H. Wu, End-to-end methane gas detection algorithm based on transformer and multi-layer perceptron, Opt. Express 32 (2024) 987–1002.
[16] S. Qiao, Y. He, H. Sun, P. Patimisco, A. Sampaolo, V. Spagnolo, Y. Ma, Ultra-highly sensitive dual gases detection based on photoacoustic spectroscopy by exploiting a long-wave, high-power, wide-tunable, single-longitudinal-mode solid-state laser, Light Sci. Appl. 13 (2024) 100.
[17] H. Wu, X. Yin, L. Dong, Z. Jia, J. Zhang, F. Liu, W. Ma, L. Zhang, W. Yin, L. Xiao, S. Jia, F.K. Tittel, Ppb-level nitric oxide photoacoustic sensor based on a mid-IR quantum cascade laser operating at 52°C, Sens. Actuators B: Chem. 290 (2019) 426–433.
[18] G. Zhang, S. Qiao, Y. He, C. Liu, Y. Ma, Multi-resonator T-type photoacoustic cell based photoacoustic spectroscopy gas sensor for simultaneous measurement of $C_2H_2$, $CH_4$, and $CO_2$, Sens. Actuators B: Chem. 427 (2025) 137168.
[19] H. Ma, Y. Chen, S. Qiao, Y. He, Y. Ma, A high sensitive methane QEPAS sensor based on self-designed trapezoidal-head quartz tuning fork and high power diode laser, Photoacoustics 42 (2025) 100683.
[20] W. Wang, H. Lv, Y. Zhao, C. Wang, H. Luo, H. Lin, J. Xie, W. Zhu, Y. Zhong, B. Liu, J. Yu, H. Zheng, Sub-ppb level HCN photoacoustic sensor employing dual-tube resonator enhanced clamp-type tuning fork and U-net neural network noise filter, Photoacoustics 38 (2024) 100629.
[21] R. Wang, S. Qiao, Y. He, Y. Ma, Highly sensitive laser spectroscopy sensing based on a novel four-prong quartz tuning fork, Opto-Electron. Adv. 8 (2025) 240275.
[22] H. Wu, X. Yin, L. Dong, K. Pei, A. Sampaolo, P. Patimisco, H. Zheng, W. Ma, L. Zhang, W. Yin, L. Xiao, V. Spagnolo, S. Jia, F.K. Tittel, Simultaneous dual-gas QEPAS detection based on a fundamental and overtone combined vibration of quartz tuning fork, Appl. Phys. Lett. 110 (2017) 121104, 1.
[23] X. Zhao, C. Li, H. Qi, J. Huang, Y. Xu, Z. Wang, X. Han, M. Guo, K. Chen, Integrated near-infrared fiber-optic photoacoustic sensing demodulator for ultra-high sensitivity gas detection, Photoacoustics 33 (2023) 100560.
[24] H. Wu, L. Dong, X. Yin, A. Sampaolo, P. Patimisco, W. Ma, L. Zhang, W. Yin, L. Xiao, V. Spagnolo, S. Jia, Atmospheric $CH_4$ measurement near a landfill using an ICL-based QEPAS sensor with V−T relaxation self-calibration, Sens. Actuators B: Chem. 297 (2019) 126753, 2.
[25] T. Liang, S. Qiao, Z. Lang, Y. Ma, Highly sensitive trace gas detection based on in-plane single-quartz-enhanced dual spectroscopy, Sensors 22 (2022) 1035.
[26] J.P. Waclawek, R. Lewicki, H. Moser, M. Brandstetter, F.K. Tittel, B. Lendl, Quartz-enhanced photoacoustic spectroscopy-based sensor system for sulfur dioxide detection using a CW DFB-QCL, Appl. Phys. B 117 (2014) 113–120.
[27] X. Yin, H. Wu, L. Dong, B. Li, W. Ma, L. Zhang, F.K. Tittel, ppb-Level $SO_2$ photoacoustic sensors with a suppressed absorption-desorption effect by using a 7.41 μm external-cavity quantum cascade laser, ACS Sens 5 (2020) 549–556.
[28] G. Cooper, E.B. Zarate, R.K. Jones, C.E. Brion, Absolute oscillator strengths for photoabsorption, photoionization and ionic photofragmentation of sulphur dioxide. I. The valence shell, Chem. Phys. 150 (1991) 237–250.
[29] K. Chung, J.G. Calvert, J.W. Bottenheim, The photochemistry of sulfur dioxide excited within its first allowed band (3130 Å) and the “forbidden” band (3700–4000 Å), Int. J. Chem. Kinet. 7 (1975) 161–182.
[30] M.A. Gondal, J. Mastromarino, Pulsed laser photoacoustic detection of $SO_2$ near 225.7 nm, Appl. Opt. 40 (2001) 2010–2016.
[31] X. Yin, L. Dong, H. Wu, H. Zheng, W. Ma, L. Zhang, F.K. Tittel, Highly sensitive $SO_2$ photoacoustic sensor for $SF_6$ decomposition detection using a compact mW-level diode-pumped solid-state laser emitting at 303 nm, Opt. Express 25 (2017) 32581–32590.
[32] B. Chen, H. Li, X. Zhao, M. Gao, K. Cheng, X. Shao, X. Yin, Trace photoacoustic $SO_2$ gas sensor in $SF_6$ utilizing a 266 nm UV laser and an acousto-optic power stabilizer, Opt. Express 31 (2023) 6974–6981.
[33] H. Wu, L. Dong, H. Zheng, X. Liu, X. Yin, W. Ma, L. Zhang, W. Yin, S. Jia, F.K. Tittel, Enhanced near-infrared QEPAS sensor for sub-ppm level $H_2S$ detection by means of a fiber amplified 1582 nm DFB laser, Sens. Actuators B. 221 (2015) 666–672.
[34] H. Wu, L. Dong, H. Zheng, Y. Yu, W. Ma, L. Zhang, W. Yin, L. Xiao, S. Jia, F. K. Tittel, Beat frequency quartz-enhanced photoacoustic spectroscopy for fast and calibration-free continuous trace-gas monitoring, Nat. Commun. 8 (2017) 15331.

**Xiaowen Shen** is now pursuing a Ph.D. degree in atomic and molecular physics in the Institute of Laser Spectroscopy of Shanxi University, China. Recently, Her research has focused on the development of gas sensors, photoacoustic spectroscopy, photothermal spectroscopy and laser spectroscopy techniques.

**Yixin Zhang** is now pursuing a Ph.D. degree in atomic and molecular physics in the Institute of Laser Spectroscopy of Shanxi University, China. Her research interests include gas sensors, photoacoustic spectroscopy, and laser spectroscopy techniques.

**Ruyue Cui** received her dual Ph.D. degrees in physics from Shanxi University, China, and Universitе du Littoral Cote d'Opale, France, in 2023. Currently, she is a lecturer at the Institute of Laser Spectroscopy at Shanxi University. Her research interests encompass optical sensors and laser spectroscopy techniques.

**Donghe Tian** graduated from Changchun University of Science and Technology in 2013 with a master's degree in optics, and has been working in Changchun New Industry Optoelectronics Technology Co. His main research interests include acousto-optic lasers and picosecond lasers.

**Ming Cheng** graduated from Changchun University of Science and Technology with a bachelor's degree in 2018. Since July 2018, She has assisted in developing solid-state lasers in Changchun New Industries Optoelectronics Technology Co., Ltd.

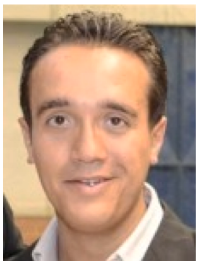

**Pietro Patimisco** obtained the Master degree in Physics (cum laude) in 2009 and the Ph.D. Degree in Physics in 2013 from the University of Bari. Since 2018, he is Assistant professor at the Technical University of Bari. He was a visiting scientist in the Laser Science Group at Rice University in 2013 and 2014. Dr. Patimisco's scientific activity addressed both micro-probe optical characterization of semiconductor optoelectronic devices and optoacoustic gas sensors. Recently, his research activities included the study and applications of trace-gas sensors, such as quartz-enhanced photoacoustic spectroscopy and cavity enhanced absorption spectroscopy in the mid infrared and terahertz spectral region, leading to several publications, including a cover paper in Applied Physics Letter of the July 2013 issue.

**Angelo Sampaolo** obtained his Master degree in Physics in 2013 and the Ph.D. Degree in Physics in 2017 from University of Bari. He was an associate researcher in the Laser Science Group at Rice University from 2014 to 2016 and associate researcher at Shanxi University since 2018. Since May 2017, he was a Post-Doctoral Research associate at University of Bari and starting from December 2019, he is Assistant Professor at Polytechnic of Bari. His research activity has included the study of the thermal properties of heterostructured devices via Raman spectroscopy. Most recently, his research interest has focused on the development of innovative techniques in trace gas sensing, based on Quartz-Enhanced Photoacoustic Spectroscopy and covering the full spectral range from near-IR to THz. His achieved results have been acknowledged by a cover paper in Applied Physics Letter of the July 2013 issue.

**Chaofeng Sun** is now pursuing a M.S. degree in optical engineering in the Institute of Laser Spectroscopy of Shanxi University, China. Recently, His research has focused on the development of photoacoustic spectroscopy, photothermal spectroscopy and laser spectroscopy techniques.

**Xukun Yin** received his Ph.D. degree in atomic and molecular physics from Shanxi University, China, in 2020. From 2018–2019, he studied as a research associate in the electrical and computer engineering department, Rice University, Houston, USA. Currently he is an assistant professor in the School of Physics and Optoelectronic Engineering of Xidian University. His research interests include optical sensors and laser spectroscopy techniques.

**Vincenzo Spagnolo** obtained the Ph.D. in physics in 1994 from University of Bari. Since 2004, he works at the Technical University of Bari, formerly as assistant and associate professor and, starting from 2018, as full Professor of Physics. Since 2019, he is vice-rector of the Technical University of Bari, deputy to technology transfer. He is the director of the joint-research lab PolySense between Technical University of Bari and THORLABS GmbH, fellow member of SPIE and senior member of OSA. His research interests include optoacoustic gas sensing and spectroscopic techniques for real-time monitoring. His research activity is documented by more than 300 publications and two filed patents. He has given more than 60 invited presentations at international conferences and workshops.

**Lei Dong** received his Ph.D. degree in optics from Shanxi University, China, in 2007. From June, 2008 to December, 2011, he worked as a post-doctoral fellow in the Electrical and Computer Engineering Department and Rice Quantum Institute, Rice University, Houston, USA. Currently he is a professor in the Institute of Laser Spectroscopy of Shanxi University. His research activities research activities are focused on research and development in laser spectroscopy, in particular photoacoustic spectroscopy applied to sensitive, selective and real-time trace gas detection, and laser applications in environmental monitoring, chemical analysis, industrial process control, and medical diagnostics. He has published more than 100 peer reviewed papers with $>$ 2200 positive citations.

**Hongpeng Wu** received his Ph.D. degree in atomic and molecular physics from Shanxi university, China, in 2017. From 2015–2016, he studied as a joint Ph.D. student in the electrical and computer engineering department and rice quantum institute, Rice University, Houston, USA. Currently he is a professor in the Institute of Laser Spectroscopy of Shanxi University. His research interests include optical sensors and laser spectroscopy techniques.